

Far-field vector-diffraction of off-axis parabolic mirror under oblique incidence*

Xia-Hui Zeng(曾夏辉)[†] and Xi-Yao Chen(陈曦曜)

Department of Physics & Electronic Information Engineering, Minjiang University, Fuzhou 350108, China

(Received 17 October 2019; revised manuscript received 3 December 2019; accepted manuscript online 7 January 2020)

Based on a full vector-diffraction theory, a detailed theoretical study is carried out, aiming at providing a clear insight into the effects of different focusing and off-axis parabola parameters on far-field vector-diffraction properties of an off-axis parabolic mirror in the presence of misalignments of the incoming beam. The physical origin of these effects is also explored. The results show that the far-field intensity profile is altered by the distortion-, coma-, and astigmatism-like aberrations, which are caused by oblique incidence rather than inherent aberrations for the off-axis configuration. The radius of 90% encircled energy also increases but does not change monotonically with incident beam size increasing, or rather, it first decreases and then increases. The focal shift strongly depends on the effective focal length and oblique incidence angle, but it is almost independent of the beam size, which affects the focusing spot patterns. The intensity distribution produces a higher astigmatic image with off-axis angle increasing. Coma-like aberration starts to become dominant with beam size increasing and results in larger curved propagation trajectory. The incident polarization also affects the intensity distribution. The variation in the Strehl ratio with oblique incidence angle strongly depends on the misalignment direction and beam size as well. In addition, we find that the difference in locus between the catacaustic and the diffraction focus in the meridian is small. But the locus of the sagittal foci is obviously different from the locus of the meridian foci and the catacaustic focus. Moreover, the peak intensity of the sagittal focus is maximum, and the ratio of the peak intensity to that in the meridian plane is approximately 1.5. Understanding these effects is valuable for assessing a practical focused intensity and describing the motion of charged particles under a strong electric field in ultraintense laser–matter interaction.

Keywords: laser beam focusing, off-axis parabolic mirror, vector-diffraction theory, oblique incidence

PACS: 42.25.-p, 42.25.Fx, 42.60.Jf

DOI: 10.1088/1674-1056/ab683e

1. Introduction

As it is well known, off-axis parabolic mirrors (OAPs) can perfectly focus a broadband collimated beam, the axis of propagation of which is parallel to the axis of revolution of the mirror, into the focal point of the mirror without any chromatic aberration within the accuracy of the ray optics, and, in this sense, they are ideal focusing devices and widely used in astronomy^[1] and laser-fusion experiments.^[2] In particular, OAPs have now become essential devices to focus ultrashort laser pulses up to relativistic intensities without the undesired nonlinear and dispersive effects induced on the pulsed beam by transmissive focusing optics,^[3] with f -numbers ranging from 1 up to ~ 20 –50 and unfocused laser beam transverse sizes (setting the OAP size) ranging from a few tens of millimeters for the TW-scale lasers up to a few hundreds of millimeters for sub-PW to PW scale systems. This relativistic laser intensity creates many exciting opportunities for laser–matter interactions.^[4,5]

However, when an OAP is irradiated by a parallel beam with oblique incidence, the reflected light rays will form a catacaustic, which is defined as either the envelope of light rays reflected by the mirror^[6] or the loci of singularities in the flux density.^[7] Early in 1964 Scarborough showed that the cata-

caustic of a two-dimensional (2D) OAP illuminated by a tilted plane wave is a circular arc lying below the tilted axis of the mirror in the framework of ray theory.^[6] Recently, Bell *et al.* further investigated that the catacaustic of a three-dimensional (3D) paraboloid illuminated by a tilted plane wave.^[8] However, researchers only concerned the geometry of the caustics and not the distribution of light intensity. In this paper, our results show that in the framework of geometrical optics, the catacaustic of an OAP can only give an approximate position of the diffraction focus in the meridian plane, but cannot give the position of the diffraction focus in the sagittal plane. And the peak intensity of the sagittal focus is maximum, and the ratio of the peak intensity to that in the meridian plane is approximately 1.5.

On the other hand, motivated by the widespread diffusion of OAP mirrors as optical devices to focus ultrashort laser pulses, a growing effort is being devoted by the community active in the field of ultraintense laser–matter interaction to the accurate calculating of the spatial structure of the electromagnetic field in the focal regions. In the case of the laser interaction with a solid target, for example, due to a pedestal and/or the picosecond prepulse, a pre-plasma can develop in front of the target surface, leading the main interaction to take place

*Project supported by the Science Foundation for Youth Scholars of Minjiang University, China (Grant No. Mj9n201602) and the National Science and Technology Major Project of the Ministry of Science and Technology of China.

[†]Corresponding author. E-mail: xiahuiz@126.com

slightly before the focal plane. To the best of our knowledge, the physical processes involved in laser–matter interaction are normally modeled by using focused pulses with an ideal space structure.^[5] Therefore, the accurate calculating of the light intensity distribution and pattern of focal spot is still important.

As matter of fact, the first paper dealing with the field intensity distribution of an OAP dates back to 1979. Based on the calculation of the catacaustic curve, Howard investigated the focusing properties of OAPs under small tilt error in the framework of ray optics.^[2] Arguijo *et al.* further pointed out that the diffraction patterns in the focal plane of an OAP for zero-field angle are altered by the aberrations that are inherent in the OAP surface: astigmatism and coma.^[9] A ray-tracing approach was taken by Arguijo and Scholl to evaluate the shape of a tilted plane wave focused by an OAP. They claimed that for a tilted beam focused by an OAP the focus is no longer point-like (with considering no diffraction effect), or rather, it is a distorted spot.^[10] It is indisputable that these researchers have presented some useful results in the framework of geometric optics or scalar diffraction theory. However, the scalar diffraction theory and geometric optics are deficient in predicting the quality of the focal spot generated by OAPs because the vector characteristics of electromagnetic field are not taken into account. For more accurately describing such a nonparaxial beam, especially when the polarization effect is considered, a vector-diffraction theory is taken as a rigorous tool.^[4,11–20] Moreover, the expressions of its electromagnetic field must satisfy Maxwell's four equations beyond the paraxial regime. As matter of fact, an earlier discussion on vector-diffraction properties may date back to 1920 when Ignatovsky obtained formulae for the electric and magnetic field vectors in the image region of a parabolic mirror (PM) of any angular aperture.^[12] Unfortunately his deductions from these formulae were chiefly restricted to the study of the energy flow across the central bright nucleus of the image. A detailed framework to analyze focused beams by using the vectorial characteristics was initiated by Stratton and Chu,^[21] in which both the electric field and magnetic field are substituted into Maxwell's equations. Another classical approach was provided by Richards and Wolf through decomposing the incident field into an angular spectrum of plane waves, by which the focused vectorial characteristics of the beam are accurately described.^[22] More recently, Labate *et al.*^[23] reported on the effects of small misalignments on the intensity and Strehl ratio (SR) for a laser beam focused by an OAP in the framework of Stratton–Chu vector-diffraction theory. However, they restricted their attention to the maximum achievable intensity and the SR in the presence of small misalignments, rather than systematically considering the effects of off-axis angle of an OAP, polarization of light and f -numbers on the focused electromagnetic vector field behavior, nor on the 3D propagation

characterization of the focused beam.

Although the ray and diffraction optics of OAP are extensively studied, a detailed knowledge of the far-field vector-diffraction field intensity distributions and the effects of off-axis angle of an OAP, the effects of polarization of light and f -numbers on the vector-diffraction properties of the focused electromagnetic field by an OAP used with an incident beam having a nonzero angle of incidence in the context of high-intensity laser–matter interaction is still missing.

In this paper, we report on a detailed theoretical study, based on a full vector-diffraction treatment, aiming at providing a clear insight into the effects of different focusing and off-axis parabola parameters normally employed in the context of intense laser–matter interaction experiments on far-field vector-diffraction properties of an OAP illuminated by a slightly tilted incoming beam. In what follows, we first use the Stratton–Chu theory to provide far-field vector-diffraction formulae suitable for calculating the intensity distribution of a super-Gaussian laser beam focused by an OAP in the presence of misalignments of the incoming beam. We then use the far-field vector-diffraction formulae derived to investigate in detail the characterization of focused vector fields formed by an OAP with a tilted plane wave. The focused vector field 3D spatial structures anywhere in the focal volume, focal shift, radius of 90% encircled energy, SR, position change of the maximum intensity and difference between our results and those based on ray optics are calculated and discussed. Finally, we draw some conclusions about the effect of slightly tilted incidence on the far-field vector-diffraction characteristics of an OAP.

2. Far-field vector-diffraction formulae

We first consider a parent paraboloid with its axis of revolution symmetry coinciding with the z axis and its focus coinciding with the origin of a Cartesian coordinate system $S(x, y, z)$. The apex of the paraboloid is in the negative z direction with a distance f to the left of the origin, as shown in Fig. 1. A point on the surface of the paraboloid is denoted by $O(x_0, y_0, z_0)$. The equation of the parent paraboloid is then given by

$$z_0 = \frac{x_0^2 + y_0^2}{4f} - f, \quad (1)$$

where f is the parent focal length. In this paper, we assume that the incident wave is reflected only once, *i.e.*, the field scattered off the surface leaves the paraboloid. The region of the parent paraboloid, made up of the OAP surface, is specified as

$$\Sigma : -a \leq x_0 - h \leq a \quad \text{and} \quad -a \leq y_0 \leq a, \quad (2)$$

where h is the distance from the z axis to the center of the incident beam and $2a$ is the greatest transverse width of the paraboloid. We call h the offset.

Next, we consider an incident beam with a planar wavefront and a super-Gaussian transverse amplitude profile, which are to be specified below. These two assumptions are of course an approximation of a real laser beam, as long as we limit ourselves to the near-field region, as a practical real case. Let the incoming beam propagate at an arbitrary angle θ with respect to the negative z direction and be linearly polarized as shown in Fig. 1. We assume that the angle θ is very small so that the small-angle approximation is adopted, *i.e.*, $\sin \theta \approx \theta$ and $\cos \theta \approx 1$. Such assumed incident fields on the paraboloidal surface are given by

$$\mathbf{E}_i = (\Psi_{0x}\hat{x} + \Psi_{0y}\hat{y}) \exp[-ik\Phi(x, y, \theta)], \quad (3)$$

$$\mathbf{H}_i = \frac{1}{\eta}(\Psi_{0y}\hat{x} - \Psi_{0x}\hat{y}) \exp[-ik\Phi(x, y, \theta)], \quad (4)$$

dropping insignificant constant-phase and time-oscillation terms. In the above equations $\eta = \sqrt{\mu/\varepsilon}$ is the intrinsic impedance of the medium, with ε and μ being the capacitvity and inductivity of the medium, respectively, k is the wave number and is given by $k = 2\pi/\lambda$, with λ being the wavelength of the incident beam, Ψ_{0x} and Ψ_{0y} represent the spatial envelopes of the light in the x and y directions, respectively, and $\Phi(x, y, \theta)$ is the aberration function. Note that the aberration here is caused by oblique incidence, not wavefront aberration of the incident beam. When the propagation axis of a collimated beam is tilted with a very small angle θ_x or θ_y with

respect to the z axis in the x - z or y - z planes [in the case of the setup shown in Fig. 1, the y axis is normal to the plane of Fig. 1(b) and the x axis lies on this plane], the aberration function is given by $x\theta_x$ or $y\theta_y$. In other words, the field distribution acquires an additional phase factor given by $\exp(-ikx\theta_x)$ or $\exp(-iky\theta_y)$ (from now on, for conciseness, we will refer to oblique incidence around x as “ θ_x ,” and similarly for y).

To calculate the field in the region near the focus of an OAP, we use the vector-diffraction formulae based on the Stratton–Chu integrals of Green’s theorem,^[21] which provides the electric and magnetic field at point $P(x_P, y_P, z_P)$ in the far field as follows:

$$\mathbf{E}(P) = \frac{1}{4\pi} \iint_{S_{\text{OAP}}} [i\omega\mu(\hat{n} \times \mathbf{H})G + (\hat{n} \times \mathbf{E}) \times \nabla G + (\hat{n} \cdot \mathbf{E})\nabla G] dA, \quad (5)$$

$$\mathbf{H}(P) = \frac{1}{4\pi} \iint_{S_{\text{OAP}}} [i\omega\varepsilon(\mathbf{E} \times \hat{n})G + (\hat{n} \times \mathbf{H}) \times \nabla G + (\hat{n} \cdot \mathbf{H})\nabla G] dA, \quad (6)$$

where ω is the angular temporal frequency of the beam, $G = \exp(ikr_{OP})/r_{OP}$, and ∇G should be used to calculate the point O and can be expressed as $-ikG(1 - 1/ikr_{OP})r_{OP}/r_{OP}$ with $r_{OP} = r_P - r_O$ and $r_{OP} = |r_{OP}|$. It is noted that the contour integral in the original Stratton–Chu integral formula is not included, because it is negligible for the continuous paraboloidal surface calculation.

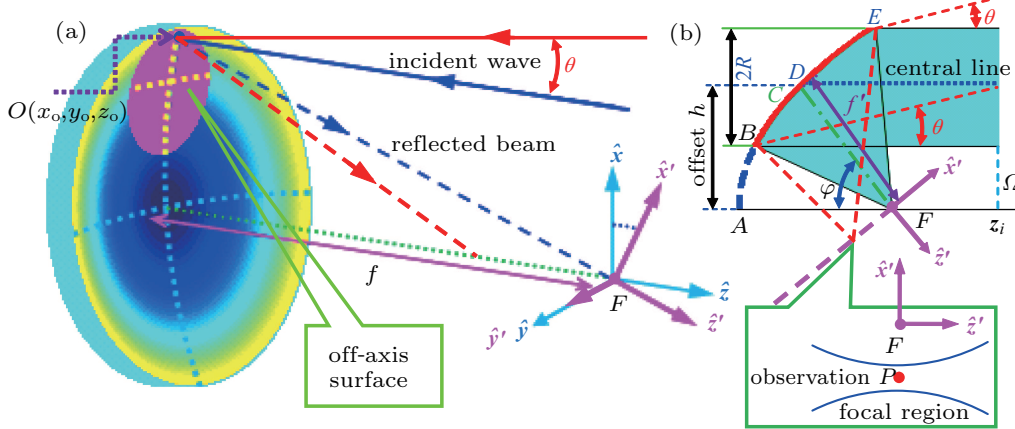


Fig. 1. Schematic illustrating reflection of OAP and sketch of Cartesian coordinate systems $Fxyz$ and $Fx'y'z'$. (a) 3D view of paraboloid reflection. (b) Meridional section of OAP. Focus F of OAP coincides with origin of Cartesian coordinate system.

The paraboloid area element dA can be written as

$$\begin{aligned} dA &= \left[1 + \left(\frac{\partial z_0}{\partial x_0} \right)^2 + \left(\frac{\partial z_0}{\partial y_0} \right)^2 \right]^{1/2} dx_0 dy_0 \\ &= \left(1 + \frac{x_0^2 + y_0^2}{4f^2} \right)^{1/2} dx_0 dy_0. \end{aligned} \quad (7)$$

The unit inward normal vector to this paraboloidal surface is expressed as

$$\hat{n}(x_0, y_0) = \frac{-(1/2f)(x_0\hat{x} + y_0\hat{y}) + \hat{z}}{\sqrt{1 + (x_0^2 + y_0^2)/4f^2}}, \quad (8)$$

where \hat{x} , \hat{y} , and \hat{z} are the unit basis vectors of the Cartesian coordinates. The electric and magnetic field appearing in Eqs. (5) and (6) are considered to be the sum of the corresponding incident and reflected field, which are boundary conditions on the OAP surface. The total electric and magnetic field are given as follows:^[11,20]

$$\mathbf{E} = \mathbf{E}_i + \mathbf{E}_r = 2\hat{n}(\hat{n} \cdot \mathbf{E}_i), \quad (9)$$

$$\mathbf{H} = \mathbf{H}_i + \mathbf{H}_r = 2\mathbf{H}_i - 2\hat{n}(\hat{n} \cdot \mathbf{H}_i). \quad (10)$$

Researchers have shown that in Cartesian coordinate system S ,

the diffraction patterns in the focal plane of an OAP for zero-field angle are altered by the aberrations that are inherent in the OAP surface, *i.e.*, astigmatism and coma.^[9,10] The factor that contributes to this behavior is the lack of symmetry that causes the wave-front reflected by the OAP surface to deform, and the optical path difference to become non-symmetric with respect to the observation plane. To avoid generating these inherent aberration effects and analyze exactly the focusing vector-electromagnetic field structure after off-axis paraboloidal reflection in the observation plane, it is useful to introduce a new Cartesian coordinate system S' (x', y', z'). Let the direction of propagation of the focusing beam reflected by the paraboloidal surface coincide with the z' axis of the new coordinate system S' as shown in Fig. 1. The new coordinate system S' is obtained by rotating the coordinate system S an angle φ around the y axis. As shown in Fig. 1(b), the rotation angle φ is defined as $\angle AFC$, where the line \overline{CF} is an angular bisector such that $\angle BFC = \angle CFE$. It is noted that the line \overline{CF} does not coincide with the line \overline{DF} connected to the center ray of the incoming beam. We choose the line \overline{CF} as the alignment axis because it gives a symmetric range of direction cosines. Owing to this symmetry, these so-called inherent aberrations of the off-axis paraboloidal surface do not exist. This result has been verified in Ref. [20]. Thus, based on the Stratton–Chu integrals of Green’s theorem the vector electromagnetic fields near the focus from the off-axis paraboloidal reflection in the S' frame can be expressed as follows:

$$E'_F(P) = \frac{ik}{2\pi} \iint_{S'_{\text{OAP}}} J \exp[ik(ux'_p + vy'_p + \gamma z'_p)] \times \exp[-ik\Phi(u, v, \theta)] dudv \times \left\{ \left[\left(\frac{1}{r_o} - \frac{x_o^2}{2fr_o^2} \right) \Psi_{0x} - \frac{x_o y_o}{2fr_o^2} \Psi_{0y} \right] \hat{x}' + \left[\left(\frac{1}{r_o} - \frac{y_o^2}{2fr_o^2} \right) \Psi_{0y} - \frac{x_o y_o}{2fr_o^2} \Psi_{0x} \right] \hat{y}' + (x_o \Psi_{0x} + y_o \Psi_{0y}) \frac{1}{r_o^2} \hat{z}' \right\}, \quad (11)$$

$$H'_F(P) = \frac{ik}{2\pi} \iint_{S'_{\text{OAP}}} \frac{J \exp[ik(ux'_p + vy'_p + \gamma z'_p)]}{\eta} \times \exp[-ik\Phi(u, v, \theta)] dudv \times \left\{ \left[\left(-\frac{x_o y_o}{2fr_o^2} \right) \Psi_{0x} + \left(\frac{x_o^2 - y_o^2}{4fr_o^2} - \frac{f}{r_o^2} \right) \Psi_{0y} \right] \hat{x}' + \left[\left(\frac{x_o^2 - y_o^2}{4fr_o^2} + \frac{f}{r_o^2} \right) \Psi_{0x} + \left(\frac{x_o y_o}{2fr_o^2} \right) \Psi_{0y} \right] \hat{y}' + (y_o \Psi_{0x} - x_o \Psi_{0y}) \frac{1}{r_o^2} \hat{z}' \right\}, \quad (12)$$

where \hat{x}' , \hat{y}' , and \hat{z}' are the unit basis vectors oriented along the new Cartesian axes x', y', z' attached to the OAP, the origin of which is positioned at the focus of the mirror, and

$$u = -(x_o \cos \varphi + z_o \sin \varphi)/r_o, \quad (13)$$

$$v = -y_o/r_o, \quad (14)$$

$$\gamma = -(-x_o \sin \varphi + z_o \cos \varphi)/r_o, \quad (15)$$

which are called direction cosines in the S' frame. The Jacobian of the transformation can be expressed as

$$J = \frac{4f^2}{\gamma(1 + u \sin \varphi + \gamma \cos \varphi)^2}. \quad (16)$$

By a series of intricate derivations, the aberration function $\Phi(u, v, \theta)$ induced by oblique incidence can be written in terms of the angular spherical coordinate as

$$\Phi(\alpha, \beta, \theta) = \theta \frac{2f \tan \alpha [-(\cos \beta \sin \varphi + \cos \varphi) + \sec \alpha]}{(\cos \beta \cos \varphi \tan \alpha - \sin \varphi)^2 + \sin^2 \beta \tan^2 \alpha} \times (\cos \beta \cos \varphi - \sin \varphi \tan \alpha), \quad (17)$$

where α and β are respectively the polar and azimuthal angle of the spherical coordinate. When φ is equal to zero (that is, the PM is in the on-axis configuration), equation (17) reduces to

$$\Phi(\alpha, \beta, \theta) = 2f\theta \tan(\alpha/2) \cos \beta. \quad (18)$$

This result is in agreement with the result of April *et al.*^[16] By expanding the function $\tan(\alpha/2)$ as a power series of $\sin(\alpha)$, we can obtain an insight into the form of this particular aberration function. Hence, the aberration function can be written as follows:

$$\Phi(\alpha, \beta, \theta) \approx f\theta \sin \alpha \cos \beta + \frac{1}{4} f\theta \sin^3 \alpha \cos \beta + \frac{1}{8} f\theta \sin^5 \alpha \cos \beta + \frac{5}{64} f\theta \sin^7 \alpha \cos \beta + \dots = f\theta g(\sin \alpha) \cos \beta. \quad (19)$$

The first term on the right-hand side of Eq. (19) corresponds to the distortion, which displaces the position of the focal spot by an amount $f\theta$ along the x axis with respect to the focus of the PM. The second term relates to the primary coma whose aberration coefficient is $f\theta/4$. Higher-order terms correspond to higher-order coma such as secondary coma, etc. Therefore, we expect that when a collimated beam is incident on a PM with a nonzero angle of incidence, the field distribution in the focal plane merely suffer distortion and coma, but not astigmatism. This conclusion will be confirmed by the following 3D intensity calculations.

When $\varphi \neq 0$ (that is, the PM is in the off-axis configuration), the aberration function (Eq. (17)) of an OAP with tilted incident beam can be qualitatively expressed as

$$\Phi(\alpha, \beta, \theta) \propto f'\theta g_1(\varphi, \beta, \sin \alpha) \cos^2 \beta + f'\theta g_2(\varphi, \beta, \sin \alpha) \cos \beta + f'\theta g_3(\varphi, \beta, \sin \alpha), \quad (20)$$

where f' is the effective focal length (EFL) of the OAP system. The first term on the right-hand side of Eq. (20) relates to the astigmatism-like aberration whose aberration coefficient is $f'\theta g_1(\varphi, \beta, \sin \alpha)$. The second term relates to the distortion- and coma-like aberrations whose aberration coefficient is $f'\theta g_2(\varphi, \beta, \sin \alpha)$.

3. Numerical calculations and discussion

The far-field vector-diffraction properties of linearly polarized collimated light focused by an OAP under oblique incidence can be analyzed based on Eqs. (11) and (12). However, the integrals appearing in Eqs. (11) and (12) have no closed form and must be calculated numerically. To estimate these numerical integrals involving rapidly oscillating terms, a Levin method is chosen.^[24] In this section, the electromagnetic field distributions will be computed for different values of the parameters that characterize the optical system and incident condition. The first parameter is the oblique angle θ of the incident beam, which can quantify the amount of aberration in the focused beam. In the following section, to clearly reveal the influence of oblique incidence on the far-field vector-diffraction properties, both θ_x and θ_y are separately introduced. The second parameter is the rotation angle φ , which quantifies the amount of the angle for off-axis paraboloidal surface deviating from on-axis configuration, and is defined as $\frac{1}{2}[\arctan((h+R)/z_{0|h+R}) + \arctan((h-R)/z_{0|h-R})]$. It should be noted that the angle is not the traditionally defined off-axis angle of the OAP, which characterizes the center position of the off-axis surface, and is defined as $\arctan[h/(f-h^2/4f)]$.^[23] However, in our case, the rotation angle φ is more suitable for describing the off-axis characterizations of the focused beam. This is because we chose the angular bisector \overline{CF} as the alignment axis, which gives a symmetric range of direction cosines in Eqs. (11) and (12). On this account, we choose and use the rotation angle φ to describe the off-axis characterizations, and from now on we will improperly use “off-axis angle” to refer to the rotation angle. The third parameter is defined as $f'/2R$, where $2R$ is the waist diameter of the incident beam. For larger values of $f'/2R$, the ratio is similar to the f -number of the optical system. Note that the f' is different from the parent focal length f of the parabolic mirror as shown in Fig. 1, which increases with off-axis angle φ increasing.^[20]

We present profiles of the electromagnetic field intensities below, which are defined as $I'_E \equiv |\mathbf{E}'|^2 = |E'_x|^2 + |E'_y|^2 + |E'_z|^2$ and $I'_H \equiv |\mathbf{H}'|^2 = |H'_x|^2 + |H'_y|^2 + |H'_z|^2$. Since high-power laser beams generally have square cross-sections,^[25] we assume that the illuminating beam has a super-Gaussian top-hat beam profile of $E_0 \exp\{-[(x-x_{\text{center}})/R_{x0}]^{2n} + (y-y_{\text{center}})/R_{y0}]^{2n}\}$, where E_0 is constant amplitude and $2R_{x0}$ and $2R_{y0}$ are the beam waists in the x and y directions, respectively. For a square beam profile, $R_{x0} = R_{y0} = R$. x_{center} and y_{center} are the transverse coordinates of the center of the incoming beam. The wavelength λ of the incident beam is $1.053 \mu\text{m}$. Unless otherwise stated, the incident wave is linearly polarized along the x direction, the beam size is $320 \text{ mm} \times 320 \text{ mm}$, and the parent focal length of the OAP is 800 mm . It is beyond the scope of this paper to discuss the optimal values of the beam size and parent focal length of the parabolic mirror.

In the following section, it will be seen that the diffraction spot in the focal plane is altered by the distortion-,

astigmatism-, and coma-like aberration. As a consequence, this spot is no longer point-like; or rather, it becomes large and splitting, even exhibiting a dark center. To quantitatively analyze a change of the diffraction-spot position in the focal plane, analogous to the concept of “center of mass,” we define the “center of electric field intensity” as

$$x'_c = \frac{\sum_{i=1}^n I_{E'_i} x'_i}{\sum_{i=1}^n I_{E'_i}}, \quad y'_c = \frac{\sum_{i=1}^n I_{E'_i} y'_i}{\sum_{i=1}^n I_{E'_i}}, \quad (21)$$

where x'_c and y'_c characterize transverse coordinates of the “center of electric field intensity.” Since we account for a change of the spot position in the Gaussian focal plane, we will improperly use the “focal shift” to refer to the “position change of center of electric field intensity” for brevity. It is noted that the focus of the focused beam by an OAP is actually not in the focal plane due to the presence of the astigmatism-like aberration. This phenomenon can be clearly seen in the following 3D intensity calculations. Owing to diffusion and splitting of the spot in the focal plane, we will use the “diameter of 90% encircled energy” to refer to the “full width at half-maximum” for quantitatively analyzing the size change of a focused spot. A similar convention was used in Ref. [26].

Figure 2 shows the contour plots of the electromagnetic field intensity distributions in the focal plane (the x' - y' plane with $z'_p = 0$) for a square super-Gaussian top-hat beam focused by OAPs with different off-axis angles under oblique incidence angle $\theta_x = 0.016^\circ$, while the corresponding plots for $\theta_y = 0.016^\circ$ are not shown for brevity. These far-field vector-diffraction intensity distributions clearly show that a tilted beam focused by an OAP produces the spatial distribution in the focal volume different from the previously known results based on scalar and ray theories.^[1,2,6,10] In the case of $R = 160 \text{ mm}$, as the off-axis angle increases, the field intensity distributions exhibit the increasing of distorted spots, which is altered by increasing distortion-, astigmatism-, and coma-like aberrations. It should be emphasized that none of these kinds of aberrations is inherent aberration for the off-axis configuration claimed by Arguijo *et al.*,^[10] but they are caused by oblique incidence. This result can be easily explained by Eq. (17): when $\theta = 0$, the aberration function $\Phi(\alpha, \beta, \theta) \equiv 0$. In addition, we find that the distortion (or tilt) displaces the position of the spot in the Gaussian focal plane by an amount $-f'\theta_x$ (or $-f'\theta_y$) along the x' axis (or y' axis, the plots of which are not shown for brevity) with respect to the focus of the OAP, where f' is the EFL, but not the the parent focal length f of the OAP system. This result is different from that in Ref. [16] due to the fact that here in this work PMs are used in the off-axis configuration. This effect is clearly visible in Figs. 3–5. In addition, it is easily seen that the width of the spot increases with off-axis angle increasing, but the corresponding maximum value of the intensity decreases.

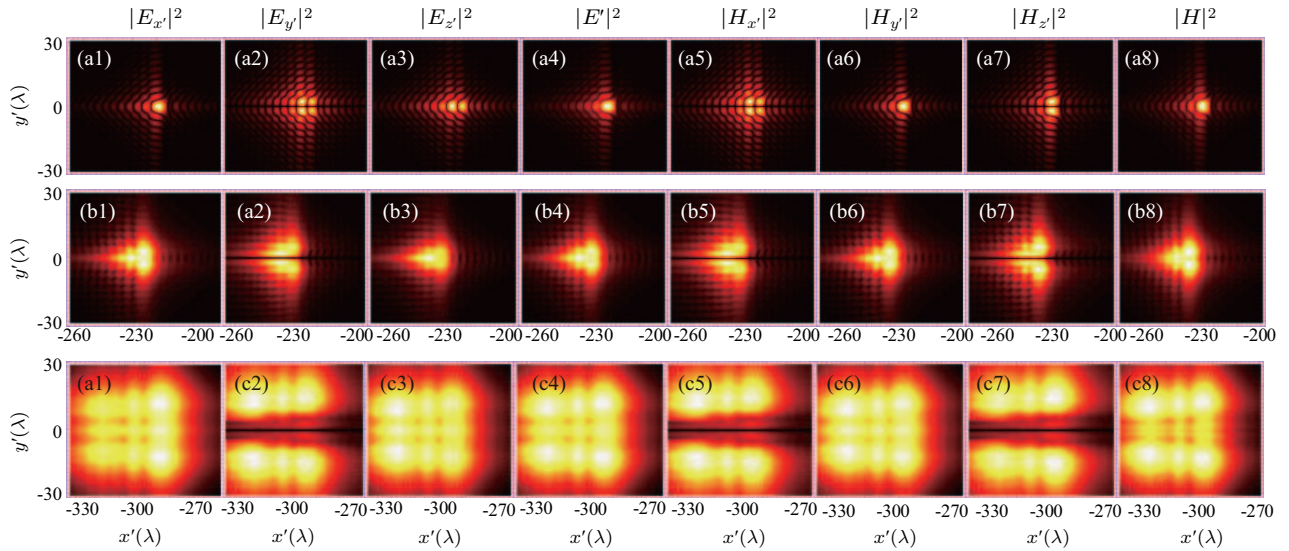


Fig. 2. Electromagnetic field intensity distributions of focused square super-Gaussian top-hat beam polarized along x direction by OAPs with off-axis angles [(a1)–(a8)] $\phi = 0^\circ$, [(b1)–(b8)] $\phi = 20.7^\circ$, and [(c1)–(c8)] $\phi = 61.6^\circ$ under oblique incidence angle of 0.016° around the x axis. Fields are computed in focal plane (the x' – y' plane with $z'_p = 0$). Intensity is indicated by “heat” of the color bar.

Figure 3(a) shows the electric field intensity distributions of the focused beam by OAPs under oblique incidence angles of $\theta_x = 0.016^\circ$ along the x' axis in the focal plane, and the plots of $d_{\text{catacaustic}}$, d_{mp} , and d_{sp} as a function of offset h . $d_{\text{catacaustic}}$ denotes the distance from the catacaustic to the origin F , d_{mp} , and d_{sp} denote the distance of diffraction foci in the meridian plane and sagittal plane to the origin F , respectively. It is easy to observe that the difference among the distance from the spot in the focal plane to the origin F , $d_{\text{catacaustic}}$, d_{mp} and d_{sp} is small when $h \leq 640$ mm ($\phi \leq 43.3^\circ$). But the difference increases with offset h increasing due to the increase of astigmatism-like aberration. Although the difference between d_{mp} and d_{sp} is subtle, practically the diffraction focus in the meridian plane does not coincide with that in the sagittal plane, and the distance between them is apparent, which will be validated later. Figure 3(b) shows the electric field intensity distributions in the focal plane for the oblique incidence angle $\theta_x = 0.01^\circ$. It is noted that the intensity maps along the x' axis with $y' = 0$ shown in Fig. 3 for each h is continuously rescaled and normalized to the corresponding maximum amplitude. This scaling allows the relatively weak intensity distribution to be plotted on the same scale as the high-intensity distribution for clarity. It is clearly observed that the width of the spot increases with h increasing, and the position deviation of the spot in the focal plane from the focus of the OAP also increases. Additionally, it can also be seen that the width of the spot and position deviation of the spot from the focus of the OAP decrease with oblique incident angle decreasing. Figure 3(c) shows that the central electric field intensity of $|E'_x|^2$ decreases and the dark center gradually appears with h increasing, until $h = 1608$ mm ($\phi = \pi/2$). Afterwards, as the value of h increases, the electric field intensity is enhanced, and the dark center gradually disappears. This similar phenomenon also happens for $\theta_x = 0.016^\circ$, which is not shown

here for brevity. Consequently, the longitudinal field $|E'_z|^2$ is predominant, and the corresponding maximum intensity ratios between the longitudinal and transverse fields in the focal plane are approximately 3×10^2 for $\theta_x = 0.016^\circ$ and 3.5×10^2 for $\theta_x = 0.01^\circ$.

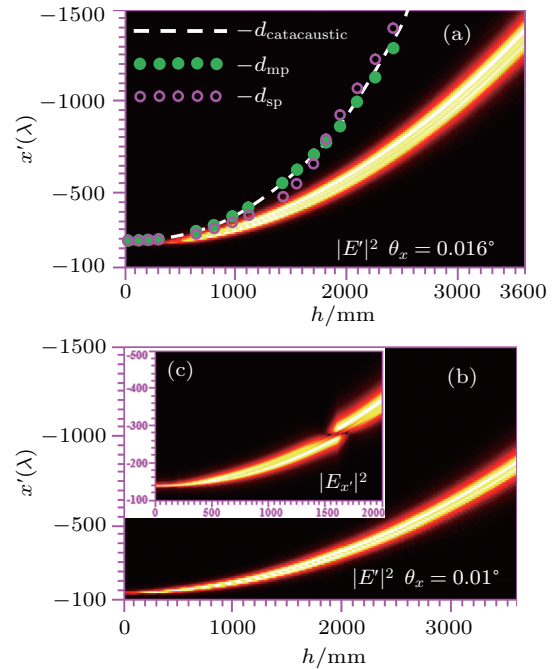


Fig. 3. Plots of $d_{\text{catacaustic}}$, d_{mp} , d_{sp} and electric field intensity distributions of focused beam by OAPs under oblique incidence angles of (a) $\theta_x = 0.016^\circ$ and (b) $\theta_x = 0.01^\circ$ along x' axis as a function of offset h . Fields are computed along x' axis with $z'_p = 0$ and $y'_p = 0$. Inset (c) shows the corresponding intensity distribution of E'_x . Intensity is indicated by color “heat”.

Figure 4 shows the effects of the oblique incidence angle and the beam size on the focused electric field intensity distributions in focal plane (x' – y' plane with $z'_p = 0$) for $\phi = 20.7^\circ$ OAP. The oblique incidence angle value ranges from 0° to 0.038° and the size of the incident beam from 100 mm to 200 mm. From the results shown in Fig. 4, it is clearly seen

that the intensity distribution of the vector field of the focused beam is deformed with respect to the intensity distribution that will be observed if the angle of incidence is zero. With a zero angle of incidence, the structure of the electric field intensity is aberration-free and it possesses lobes of relatively weak amplitude surrounding a central high-amplitude peak. When the angle of incidence is different from zero, the bilateral symmetry exhibited in the intensity distribution of a beam focused with a zero angle of incidence is destroyed by the formation of asymmetrical rings, showing a comatic image flaring in the x' direction; these distributions, characterized by a comet-like shape, confirm the presence of coma-like aberration in the focal spot when the beam is incident on the OAP with a nonzero

angle of incidence, however small it is. As the oblique incidence angle increases, an extended tail develops in the intensity profile, especially for large values of R . This effect may result from the coma- and astigmatism-like aberrations, which can be seen below. The presence of comatic aberration in the system yields a positional displacement and a modification of the width of the maximum intensity accompanied by, in most cases, a reduction of the maximum intensity. This displacement of the maximum intensity is mainly explained by the presence of distortion in the aberration function of the system; the extra amount of displacement can be attributed to the presence of coma and astigmatism in the aberration function of the system. These behaviors are verified by Fig. 5.

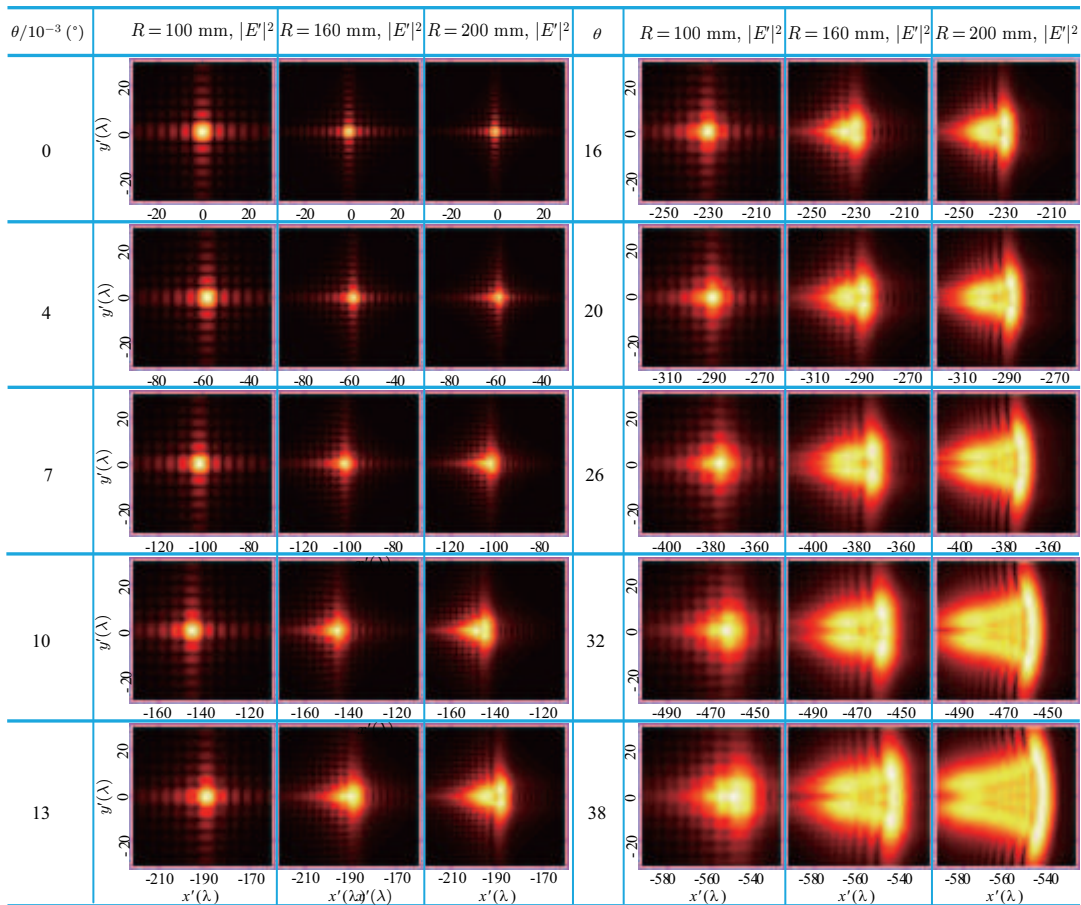


Fig. 4. Contour plots of focused electric field intensity distributions in focal plane for a $\varphi = 20.7^\circ$ OAP under different oblique incidence angles. Intensity is indicated by color “heat”.

The displacement of the center of electric field intensity (referred to as focal shift for brevity) is shown in Fig. 5(a). With a nonzero value of θ_x (or θ_y , none of the plots of which is shown here for conciseness), the electric field intensity profile is shifted in one direction with respect to the origin. The focal shift strongly depends on the amount of distortion (or tilt), but it is almost independent of the size of the incident beam. However, the size of the incident beam affects the focusing spot patterns. Consequently, the larger incident-beam size results in a larger and more split spot. By fitting the plots of Fig. 5(a),

we find that the position of the center of electric field intensity in the focal plane is approximately located at $x'_c = -f'\theta_x$ and $f' = 827.2$ mm for the OAP with $\varphi = 20.7^\circ$. Similar trends are found for θ_y and $y'_c = -f'\theta_y$, measured along the x' axis (or y' axis) with respect to the focal point of the OAP. Additionally, as seen clearly from Fig. 5(a), the radius of 90% encircled energy of the spot in the focal plane is affected not only by the angle of incidence of the beam on the OAP, but also by the size of the incident beam. The radius of 90% encircled energy increases with the value of tilt angle θ increasing for a given

R but does not change monotonically with the size R of the incident beam; or rather, it first decreases and then increases as the size of the incident beam increases. Note that this behavior can be clearly observed in Fig. 6.

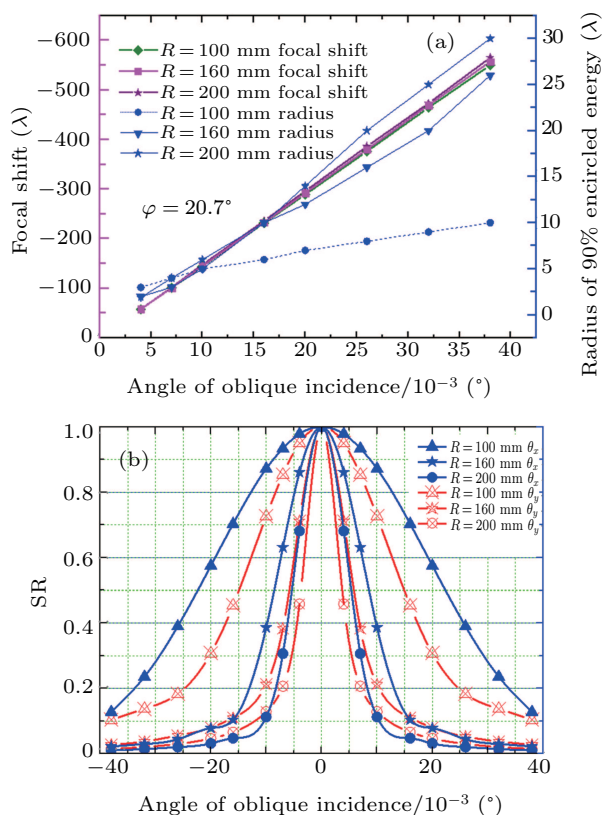


Fig. 5. Plots of (a) focal shift (position of maximum intensity) and radius of 90% encircled energy, and (b) SR of electric field intensity in the focal plane for OAP with off-axis angle $\varphi = 20.7^\circ$ versus oblique incidence angle for different R values.

The SR is the ratio of the observed maximum intensity in the focal plane to the peak intensity of the aberration-free version of the system, *i.e.*, when $\theta = 0$. Figure 5(b) shows the behaviors of SR in the case of an OAP with an off-axis angle $\varphi = 20.7^\circ$ for different R values. These plots as a function of the angle of oblique incidence are symmetric with respect to $\theta_x = 0$ or $\theta_y = 0$. For $R = 200$ mm, the SR decreases relatively quickly with the increase in θ value; for $R = 160$ mm, the SR decreases, but slowly, and for $R = 100$ mm, the SR decreases more slowly. This effect is due to the fact that a larger R results, at a given off-axis angle, in a higher coma. In addition, we observe that the decrease of the SR as a function of oblique incidence angle is faster for θ_y than for θ_x .

In our previous work,^[20] we have confirmed that the focusing performance of an OAP system without any aberration is determined by its f -number if it is illuminated exactly along the system axis. The width of the focal spot of the focused beam decreases with f -number decreasing, until it reaches the diffraction limit; that is, smaller f -number values lead to a tighter focus. However, when the angle of incidence is different from zero, the width of the spot in the focal plane does not

change monotonically with the increase of f -number (approximately equal to $f'/2R$) of the OAP system. In other words, the f -number is not suitable to characterizing the focusing performance of an OAP system with a tilted incident beam. Figure 6 shows the contour plots of the focused electric field intensity distributions along the x' axis with $z'_p = 0$ and $y'_p = 0$ for OAPs with $\varphi = 20.7^\circ$ and $\varphi = 61.6^\circ$ under the oblique incidence angle of $\theta_x = 0.016^\circ$ versus $f'/2R$, with f' fixed. It can be clearly observed that whatever the value of the off-axis angle, the width of the spot in the focal plane first decreases and then increases with incident-beam size increasing; this is a consequence of the contribution of diffraction effect and coma. However, the position of the center of electric field intensity in the focal plane is always approximately located at $x'_c = -f'\theta_x$.

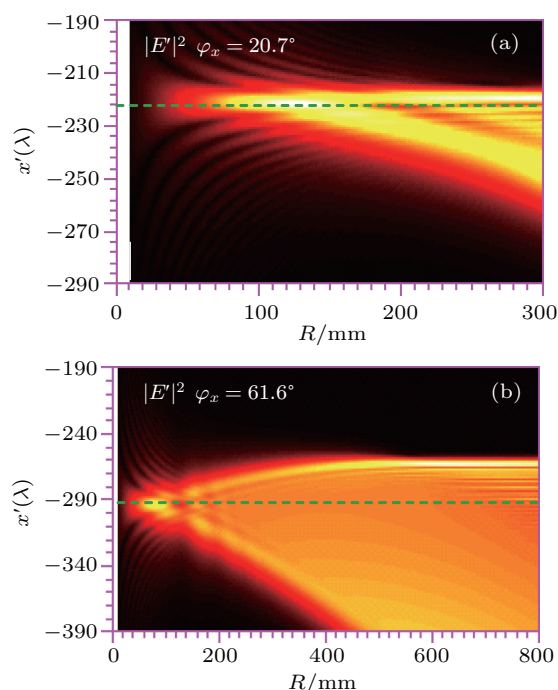


Fig. 6. Contour plots of focused electric field intensity distributions along x' axis with $z'_p = 0$ and $y'_p = 0$ for OAPs with off-axis angle of (a) $\varphi = 20.7^\circ$ and (b) $\varphi = 61.6^\circ$ under tilted incidence of $\theta_x = 0.016^\circ$ versus parabola f -number ($f'/2R$, f' is fixed). Dashed lines present center position of electric field intensity. Intensity is indicated by color “heat”.

To comprehensively understand the far-field vectorial diffraction properties of the OAP under tilted incidence, we run lots of 3D intensity calculations, which are partially shown in Figs. 7–8 for brevity. The far-field intensity distributions in the $x'-z'$ and $y'-z'$ planes and cross-section ($x'-y'$ plane) with different values of z' before and after the focal plane ($z' = 0$), are exhibited. Figure 7 presents the 3D intensity profile of the total diffraction electric field E' focused by the on-axis PM under the incident beam with $R = 160$ mm and $\theta_x = 0.016^\circ$. The intensity distribution exhibits a caustic curve in the meridional plane and plane symmetry with respect to the plane containing the diffraction focus with a displacement of $x'_c = -f'\theta_x = -212\lambda$, and the focus merely shifts perpendicularly to the optical axis. This figure clearly reveals the pres-

ence of distortion and strong coma, but the absence of astigmatism. These results can be easily explained by Eq. (19): when a collimated beam is incident on a PM with a nonzero angle of incidence, the field distribution in the focal plane merely suffers distortion and coma, but not from astigmatism. Interestingly, the tightly confined main intensity feature of the axially asymmetric focused beam propagates along a curved trajectory. This curved propagation phenomenon, analogous to the propagation of an Airy beam, can result from the cubic phase

modulation.^[27] The coma aberration is of cubic phase^[28] and results in curved propagation of the main intensity. When the off-axis angle φ is different from zero, the diffraction focus of the focused beam in the meridian plane does not coincide with that in the sagittal plane as shown in Fig. 8. As is well known, astigmatism corresponds to a difference in focus position between the sagittal and meridian plane. Figure 8 manifests the presence of astigmatism. As the off-axis angle φ increases, the intensity distribution produces a higher astigmatic image.

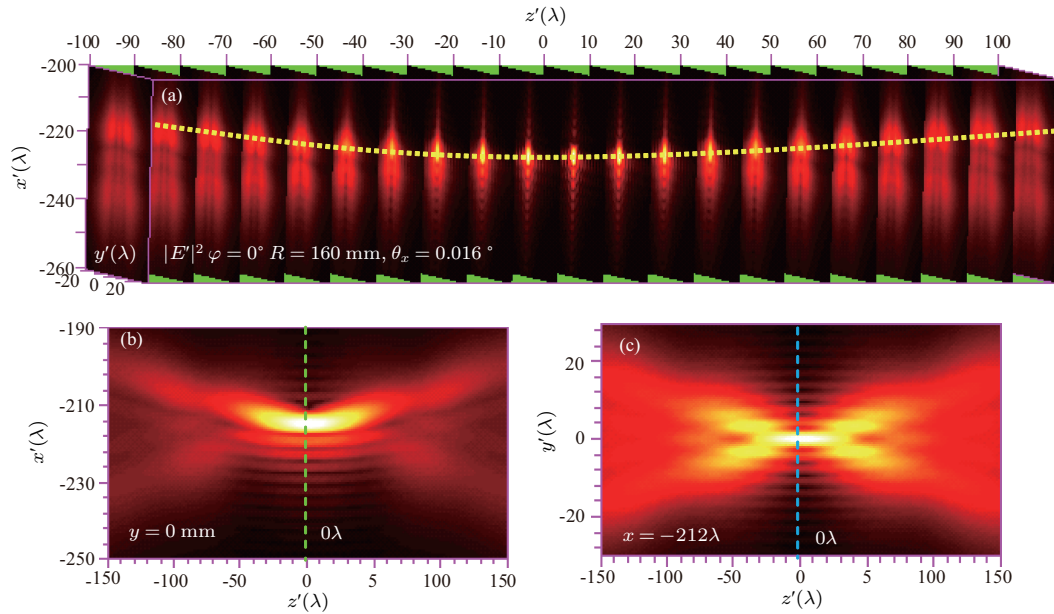


Fig. 7. 3D intensity distribution of total diffraction electric field E' focused by OAP with $\varphi = 0^\circ$ for $R = 160$ mm and $\theta_x = 0.016^\circ$. (a) Intensity profiles in cross-sections at $z = -100\lambda - 100\lambda$. (b) Intensity profile in meridional ($x'-z'$) plane. (c) Intensity profile in sagittal ($y'-z'$) plane. Bent yellow dotted line presents propagation locus of main intensity. Green and light blue dashed lines present diffraction focus position in corresponding plane. Intensity is indicated by color “heat”.

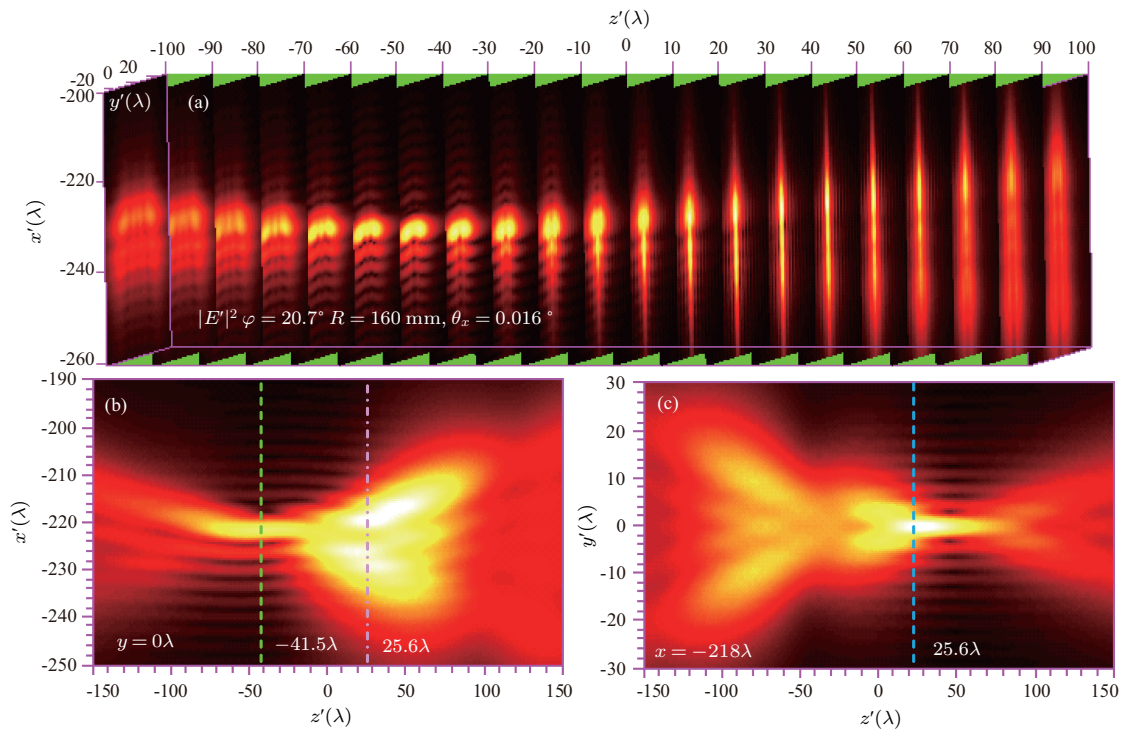


Fig. 8. 3D intensity distribution of E' focused by OAP with $\varphi = 20.7^\circ$ for $R = 160$ mm and $\theta_x = 0.016^\circ$. (a) Intensity profiles in cross-section. (b) Intensity profile in meridional plane. (c) Intensity profile in sagittal plane. Dashed lines present focus position in corresponding plane, and dashed-dotted line presents position of peak intensity. Intensity is indicated by color “heat”.

To make a comparison of numerical results in the framework between ray optics and full vector-diffraction theory, we run lots of 3D intensity distribution calculations and show loci of the catacaustic, diffraction foci in the meridian and sagittal plane for OAPs with $R = 160$ mm and $\theta_x = 0.016^\circ$ varying with the off-axis angle φ in Fig. 9. The locus of the caustic is determined by $d_{\text{catacaustic}} = f\theta \sec^3(\varphi/2)$ and $\psi = 3\varphi/2 - \pi/2$ in the framework of ray optics. The intensity distributions and loci of the diffraction foci in the meridian and sagittal planes are obtained based on Eqs. (11) and (12). From these results shown in Fig. 9 it follows that the difference between the caustic focus and the diffraction focus in the meridian plane is small, especially for $\varphi \leq 61.6^\circ$. This observation can be explained by the fact that the caustic curve is obtained under 2D OAPs, *i.e.*, it contains the singularities in the flux density in the meridian plane. But this difference is apparent with increasing φ due to the increasing of coma-like aberration. In addition, due to the presence of astigmatism-like aberration, the locus of the diffraction foci in the sagittal plane is obviously different from the other two. Moreover, we notice that the intensity of diffraction focus in the sagittal plane is maximum due to the present of astigmatism- and coma-like aberration. The peak intensity ratio of the diffraction focus in sagittal plane to that in meridian plane is approximately 1.5.

Finally, to clearly understand the effect of the incident polarization, misalignment direction and beam size on the far-field vectorial diffraction properties of the OAP under tilted incidence, we plot the 3D intensity distribution of E' focused

by OAP with $\varphi = 20.7^\circ$ for $R = 260$ mm, $\theta_x = 0.016^\circ$ and $R = 160$ mm, $\theta_y = 0.016^\circ$, while the corresponding plot for the y -polarization is not shown here for brevity. By comparing the results shown in Fig. 8 with those in Fig. 10, we can find that coma starts to become dominant with the increase of incident-beam size, and thus resulting in larger curved trajectory. Owing to asymmetric shape of the OAP, the 3D intensity distribution of E' for $\theta_y = 0.016^\circ$ is very different from that for $\theta_x = 0.016^\circ$, which has two equidistant foci in the meridional plane or sagittal plane as shown in Fig. 11. This is also a reason why the decrease of SR with oblique incident angle is faster for θ_y than for θ_x . In addition, we find that although the beam polarization can affect the focused intensity distribution, the difference between the x - and y -polarizations is small.

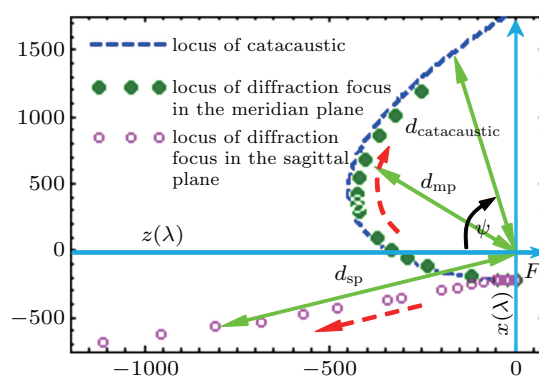


Fig. 9. Loci of the catacaustic, diffraction foci in the meridian and sagittal planes for OAPs with $R = 160$ mm and $\theta_x = 0.016^\circ$ varying with off-axis angle.

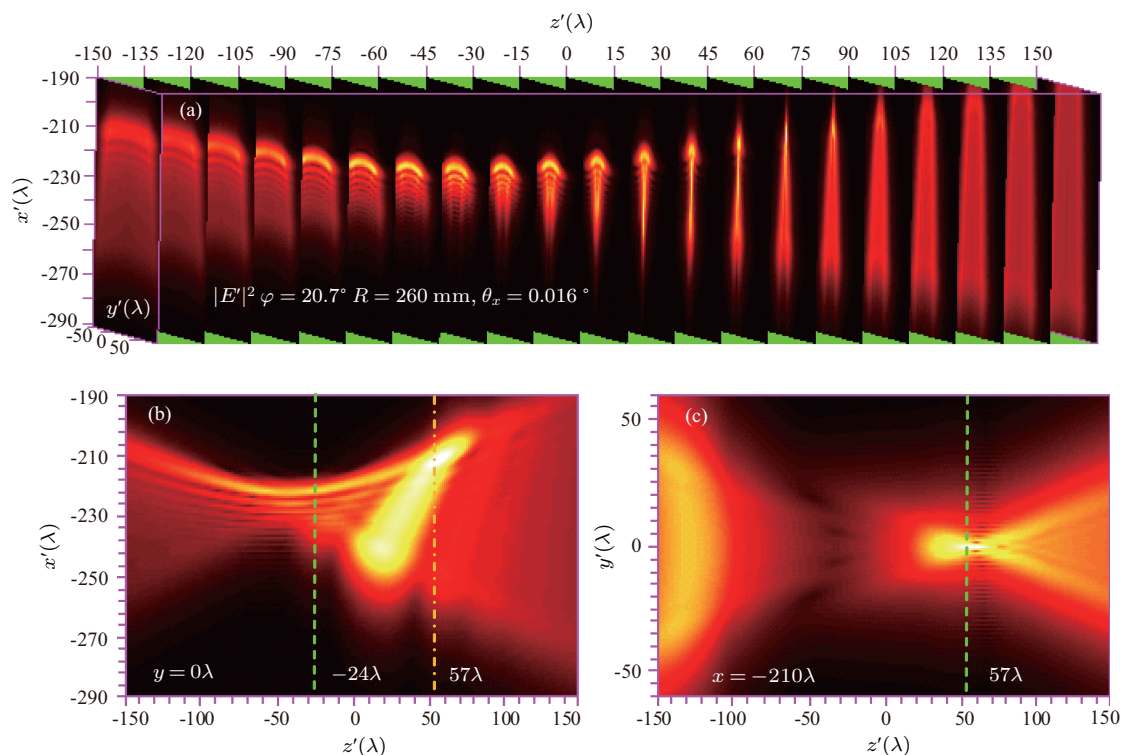


Fig. 10. 3D intensity distribution of E' focused by OAP with $\varphi = 20.7^\circ$ for $R = 260$ mm and $\theta_x = 0.016^\circ$. (a) Intensity profiles in cross-section. (b) Intensity profile in meridional plane. (c) Intensity profiles in sagittal plane. Dashed lines present focus position in corresponding plane, and dashed-dotted line presents position of peak intensity. Intensity is indicated by color “heat”.

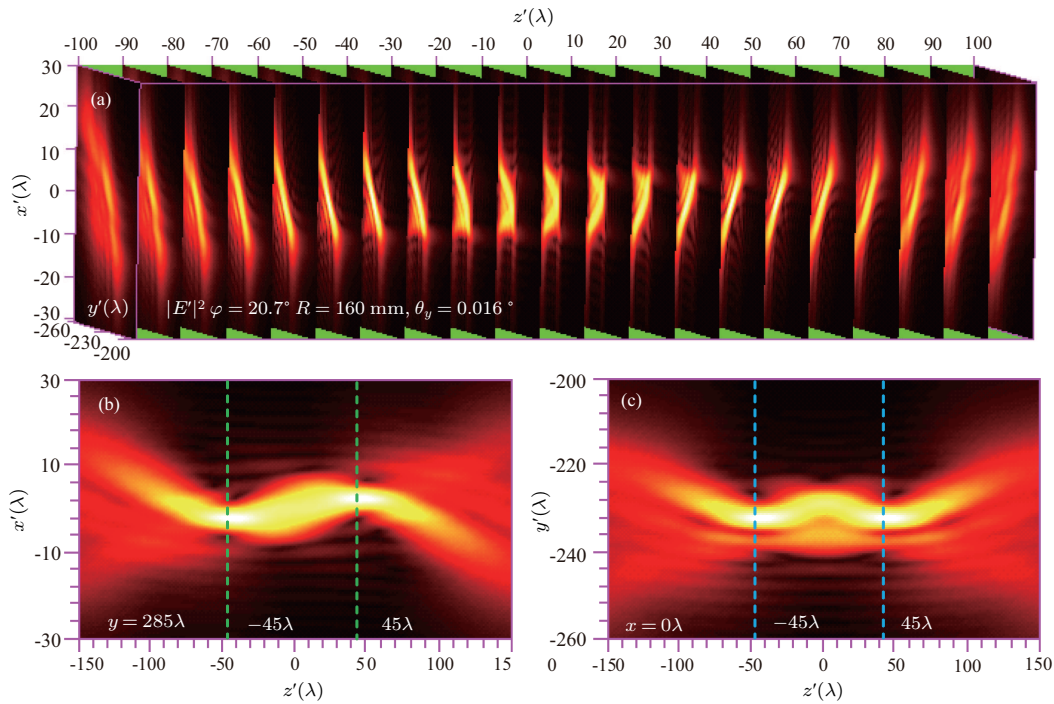


Fig. 11. 3D intensity distribution of E' focused by OAP with $\varphi = 20.7^\circ$ for $R = 160$ mm and $\theta_y = 0.016^\circ$. (a) Intensity profiles in cross-section. (b) Intensity profile in meridional plane. (c) Intensity profile in sagittal plane. Dashed lines present focus positions in corresponding planes. Intensity is indicated by color “heat”.

4. Conclusions

In this paper, we present a method to quantitatively analyze the effects of oblique incidence on the far-field vector-diffraction properties of an OAP based on a full vector-diffraction treatment. The physical origin of these effects is explored. The method described here allows the 3D intensity profiles in the focal volume, including the focused beam longitudinal profiles in the meridional and sagittal plane and transverse profiles at a generic plane, to be evaluated numerically. The focal shift, radius of 90% encircled energy, SR, polarization effect, and a position change of the maximum intensity are calculated and discussed in detail. Even though the discussion here is limited to square pupils only, this method is well suited to study circular apertures.

In conclusion, in the framework of a full vector diffraction theory, besides that all known conclusions based on ray-tracing approach are verified, we observe some interesting results. When an OAP illuminated with a tilted parallel beam, the far-field intensity distribution is altered by the distortion-, coma- and astigmatism-like aberrations, which are caused by oblique incidence rather than inherent aberrations for the off-axis configuration. The bilateral symmetry exhibited in the intensity distribution of a beam focused with a zero angle of incidence is destroyed by the formation of asymmetrical rings. A positional displacement of the spot, a change of radius of 90% encircled energy, and an SR decrease are observed. The distortion-like aberration makes the intensity profile shift in the focal plane in one direction with respect to the geomet-

ric focus of the OAP. The focal shift strongly depends on the effective focal length and oblique incidence angle, but it is almost independent of incident beam size, which affects the focusing spot patterns. The presence of coma-like aberration yields a positional displacement and an alteration of the width of the maximum intensity accompanied by a reduction of the maximum intensity, and makes the tightly confined main intensity feature of the axially asymmetric focused beam propagate along a curved trajectory. Owing to the aberration of astigmatism-like, the maximum intensity is not in the focal plane. The intensity distribution produces a higher astigmatic image with the increase of off-axis angle. Coma starts to become dominant with the increase of incident-beam size and results in more greatly curved propagation trajectory. The polarization of light slightly affects the intensity distribution. The decrease of the sensitivity of SR with oblique incidence angle is faster for misalignment in the y -direction than in the x -direction. As the oblique incidence angle increases, an extended tail develops into the intensity profile, and the width of the spot and the position deviation of the spot from the focus of the OAP increase. The radius of 90% encircled energy also increases but does not change monotonically with the size of the incident beam; or rather, it first decreases and then increases. When the off-axis angle is approximately $\pi/2$, the longitudinal field is predominant, but the maximum peak intensity ratio between the longitudinal field and transverse field in the focal plane decreases with oblique incidence angle increasing.

In addition, comparing our results with those in the framework of ray optics, we find that the difference in lo-

cus between the caustic focus and the diffraction focus in the meridian plane is small. But the locus of the diffraction foci in the sagittal plane is obviously different from that in the meridian plane and the catacaustic. Moreover, we notice that the intensity of diffraction focus in the sagittal plane is maximum. The peak intensity ratio of the diffraction focus in sagittal plane to that in meridian plane is approximately 1.5. Understanding these effects is valuable for assessing a practical focused intensity and describing the motion of charged particles under a strong electric field in ultraintense laser–matter interaction, which, in particular, is helpful in designing the ultrashort and ultraintense laser–matter interaction experiments.

Acknowledgment

We thank Prof. Liejia Qian and Prof. Guoqiang Xie at Shanghai Jiao Tong University for their encouragement of this work.

References

- [1] Wilson R N 2004 *Reflecting Telescope Optics* (Heidelberg: Springer)
- [2] Howard J E 1979 *Appl. Opt.* **18** 2714
- [3] Jeong T M, Weber S, Garrec B L, Margarone D, Mocek T and Korn G 2015 *Opt. Express* **23** 11641
- [4] Leemans W P, Nagler B, Gonsalves A J, Toth Cs, Nakamura K, Geddes C G R, Esarey E, Schroeder C B and Hooker S M 2006 *Nat. Phys.* **2** 696
- [5] Macchi A, Borghesi M and Passoni M 2013 *Rev. Mod. Phys.* **85** 751
- [6] Scarborough J B 1964 *Appl. Opt.* **3** 1445
- [7] Shealy D L and Burkhard D G 1973 *Opt. Acta* **20** 287
- [8] Bell C G, Ockendon H and Ockendon J R 2010 *J. Opt.* **12** 065703
- [9] Arguijo P, Scholl M S and Paez G 2001 *Appl. Opt.* **40** 2909
- [10] Arguijo P, Scholl M S 2003 *Appl. Opt.* **42** 3284
- [11] Bank S W, Rousseau P, Planchon T A, Chvykov V, Kalintchenko G, Maksimchuk A, Mourou G A and Yanovsky V 2005 *Appl. Phys. B* **80** 823
- [12] Ignatovsky V S 1920 *Trans. Opt. Inst. Petrograd* 1 paper 5
- [13] Varga P and Török P 2000 *J. Opt. Soc. Am. A* **17** 2081
- [14] Stadler J, Stanciu C, Stupperich C and Meixner A J 2008 *Opt. Lett.* **33** 681
- [15] April A and Piché M 2010 *Opt. Express* **18** 22128
- [16] April A, Bilodeau P and Piché M 2011 *Opt. Express* **19** 9201
- [17] Shibata K, Takai M, Uemoto M and Watanabe S 2015 *Phys. Rev. A* **92** 053806
- [18] Peatross J, Berrondo M, Smith D and Ware M 2017 *Opt. Express* **25** 13990
- [19] Chen R, Chen Z, Gao Y, Ding J and He S 2017 *Laser Photon. Rev.* **11** 1700165
- [20] Zeng X and Chen X 2019 *Opt. Express* **27** 1179
- [21] Stratton J A and Chu L J 1939 *Phys. Rev.* **56** 99
- [22] Richards B and Wolf E 1959 *Proc. Roy. Soc. A* **253** 358
- [23] Labate L, Ferrara P, Fulgentini L and Gizzi L A 2016 *Appl. Opt.* **55** 6506
- [24] Levin D 1996 *J. Comput. Appl. Math.* **67** 95
- [25] LaFortune K N, Hurd R L, Fochs S N, Rotter M D, Pax P H, Combs R L, Olivier S S, Brase J M and Yamamoto R M 2007 *Proc. SPIE* **6454** 1
- [26] Vallone G, Parisi G, Spinello F, Mari E, Tamburini F and Villoreasi P 2016 *Phys. Rev. A* **94** 023802
- [27] Polynkin P, Kolesik M, Moloney J V, Siviloglou G A and Christodoulides D N 2009 *Science* **324** 229
- [28] Mahajan V N and Dai G 2007 *J. Opt. Soc. Am. A* **24** 2994